Skutterudite unicouple characterization for energy harvesting applications

Submitted to ADVANCED ENERGY MATERIALS

DOI: 10.1002/aenm.((please add manuscript number))
Full Paper:

Skutterudite unicouple characterization for energy harvesting applications

Andrew Muto, Jian Yang, Bed Poudel, Zhifeng Ren, and Gang Chen**

Dr. Andrew Muto, Prof. Gang Chen
Department of Mechanical Engineering, Massachusetts Institute of Technology 77 Mass Ave MIT, rm 3-260, Cambridge MA 02139, USA
E-mail: andymuto@mit.edu

Dr. Jian Yang, Dr. Bed Poudel
GMZ Energy 11 Wall St, Waltham MA 02453, USA
Email: info@gmzenergy.com

Prof. Zhifeng Ren,
Dept. of Physics, Boston College, Higgins Hall 230G, Chestnut Hill MA 02467, USA
E-mail: renzh@bc.edu

Prof. Gang Chen,
Department of Mechanical Engineering, Massachusetts Institute of Technology 77 Mass Ave MIT, rm 3-260, Cambridge MA 02139, USA
E-mail: gchen2@mit.edu

Keywords: device; energy conversion; energy harvesting; skutterudite; solar; thermoelectric;

Skutterudites are promising thermoelectric materials for their high figure of merit, *ZT*, and good thermomechanical properties. In this work, we report the effective figure of merit, ZT_{eff}, and the efficiency of skutterudite legs and a unicouple working under a large temperature difference. The p- and n-type legs were fabricated with electrodes sintered directly to the skutterudite during a hot pressing process. $CoSi_2$ was used as the electrode for the n-type ($Yb_{0.35}Co_4Sb_{12}$) and Co_2Si for the p-type ($NdFe_{3.5}Co_{0.5}Sb_{12}$) skutterudites. A technique was developed to measure the ZT_{eff} of individual legs and the efficiency of a unicouple. We report an ZT_{eff}=0.74 for the n-type legs operating between 52 °C and 595 °C and an ZT_{eff}=0.51 for the p-type legs operating between 77 °C and 600 °C. The efficiency of a *p-n* unicouple was determined to be 9.1% operating between ~70 °C and 550 °C.

1. Introduction

Thermoelectric energy conversion devices are attractive because they have no moving parts, are capable of high power densities, scalable in size, and potentially highly reliable.[1] They can be used to improve the overall efficiency of existing systems by recovering waste heat, for example from vehicle exhaust, and to develop new systems such as solar thermoelectric energy converters.[2-4] The performance of a thermoelectric material is characterized most commonly by its dimensionless figure of merit, $ZT = S^2T/\rho k$ where $S(T)$, $\rho(T)$, $k(T)$ are the temperature-dependent Seebeck coefficient, electrical resistivity, and thermal conductivity, respectively, and T is the absolute temperature. If the material properties are independent of temperature then the maximum efficiency of a thermoelectric leg can be expressed as [5]

$$\eta_{\max} = \frac{T_{Hot} - T_{Cold}}{T_{Hot}} \frac{\sqrt{1+Z\overline{T}} - 1}{\sqrt{1+Z\overline{T}} + \frac{T_{Cold}}{T_{Hot}}}, \quad (1)$$

where T_{Hot} is the hot side temperature, T_{Cold} is the cold side temperature, and $\overline{T}$ is the arithmetic average of T_{Cold} and T_{Hot}.

The efficiency of real devices can differ significantly from **Eq. (1)** due to the following reasons. First, thermoelectric properties are temperature-dependent and can vary significantly from the hot side to the cold side. This is especially true for power generation applications when the hot and the cold side temperature difference spans several hundred degrees. Second, non-ideal factors such as electrical and thermal contact and spreading resistances, and heat losses at the side walls of the legs degrade the device efficiency.[6,7] Although materials' *ZT* are often reported, thermoelectric device testing is needed to link the materials to their applications and to validate the *ZT* measurements.

A major challenge for device testing is to make electrical contacts to thermoelectric legs. Because thermoelectric legs used in devices usually have a high electrical conductivity and a small length in the current flow direction, the overall resistance of the leg itself is small, which requires very small electrical contact resistances between the electrodes and the

thermoelectric materials. Other key difficulties are thermal stresses, parasitic thermal resistances, and chemical stability. Needless to say, a careful energy balance is needed to report device efficiency. Partially due to these difficulties, there are far fewer reports on device performance than materials' *ZT* values. A few groups have reported device work in the past. The thermoelectric efficiency of radioisotope generators (RTG) employed on current US space missions is 8%. These generators use SiGe legs that operate between 300 °C and 1000°C.[8] The SiGe legs are coated with Si_3N_4 and wrapped in quartz yarn to reduce sublimation. High temperature modules are prone to sublimation and oxidation, and must be encapsulated in most cases. Kambe *et al*. encapsulated a high temperature SiGe module in a stainless steel container which was evacuated and fit with compliant solder-infiltrated pads for improved heat transfer.[9] D'Angelo *et al.* tested PbTe-Bi_2Te_3 based segmented-leg modules (47 couples) from Tellurex.[10] The modules operated between 39 °C and 397 °C, the measured efficiency was 6.56% compared to the modelled efficiency of 9.8% which neglected thermal losses and contact resistances. Salzgeber *et al.* reported on the progress of skutterudite material, heat exchanger design, module intregration, and cost estimates for automotive applications.[11] El-Genk *et al.* measured the efficiency of skutterudite unicouples with bonded metallic electrodes of unspecified compostition.[12-14] The unicouple operated between 29 °C and 697 °C for hundreds of hours and demonstrated a peak efficiency of 7.3% and was calculated to be as high as 10.7% if sidewall thermal losses were eliminated. The following coatings were investigated to suppress Sb sublimation at the hot side of the legs: Ta, Ti, Mo, V.[15] Researchers at the Shanghai Institute of Ceramics have successfully bonded skutterudites to several electrode materials including Mo, Cu-Mo, and Cu-W using a Ti bonding layer.[16-19] They have also built a skutterudite module and demonstrated an efficiency of 6.4% when the device operated between 47 °C and 537 °C.[20]

In this work, we develop a platform to measure skutterudite unicouple performance when it is subjected to a large temperature difference, including the ZT_{eff} of the *n*- and *p*-type

materials and the efficiency of a *p-n* unicouple. The hot side temperature reached up to 600 °C. The skutterudite legs were made by powder metallurgy processes. Electrodes were bonded directly to the skutterudite legs. Parasitic electrical contact resistances and heat losses are carefully accounted for. We demonstrate a heat to electricity conversion efficiency among the highest ever measured for a skutterudite unicouple.

2. Effective Properties

The thermoelectric properties, $S(T)$, $\rho(T)$, $k(T)$ are usually measured independently over a small temperature difference ΔT, usually less than 10 °C. Real devices work under a much larger temperature difference. Relevant device properties are the Seebeck voltage V_S, hot side heat transfer Q_{Hot}, and the electrical resistance R. For each leg working under a large ΔT and open-circuit condition, we define effective properties, using subscript "eff", as

$$S_{eff}\left(T_{Hot},T_{Cold}\right)=\frac{-V_S}{\Delta T}=\frac{\int_{T_{Cold}}^{T_{Hot}} S(T)dT}{\Delta T}, \tag{2}$$

$$k_{eff}\left(T_{Hot},T_{Cold}\right)=Q_{Hot}\frac{L}{A\Delta T}=\frac{\int_{T_{Cold}}^{T_{Hot}} kdT}{\Delta T}, \tag{3}$$

$$\rho_{eff}\left(T_{Hot},T_{Cold}\right)=R\frac{A}{L}=\frac{\int_{T_{Cold}}^{T_{Hot}} k\rho dT}{\int_{T_{Cold}}^{T_{Hot}} kdT}. \tag{4}$$

The first equality in the above three equations defines the effective properties. Experimentally, we can measure each quantity in these definitions and thus determine the effective properties experimentally. We can combine these properties to define an effective ZT,

$$ZT_{eff} = \frac{S_{eff}^2 \overline{T}}{\rho_{eff} k_{eff}} = \frac{V_S^2 \overline{T} / |\Delta T|}{RQ_{Hot}}, \quad (5)$$

for each temperature range of T_{Cold} and T_{Hot} to which the device is subjected. We have shown in previous work that ZT_{eff} can be used in Eq. (1) to calculate the maximum conversion efficiency for Bi_2Te_3 working under 200 °C. [21]

The last equality in Eqs. (2-4) provides a way to calculate the effective properties based on the temperature-dependent transport properties of the materials. These equalities are valid when heat and charge flowing through the devices are one-dimensional and radiation heat loss from side walls is negligible. If radiation heat loss is not negligible—which is the case for our devices due to high-temperature operation—we solve the following one-dimensional differential equation,[22]

$$A\frac{d}{dx}\left(k\frac{dT}{dx}\right) - I_{TE}T\frac{dS}{dx} + I_{TE}^2\frac{\rho}{A} - \varepsilon\sigma_{sb}W\left(T^4 - T_\infty^4\right) = 0, \quad (6)$$

where A is the cross-sectional area of the thermoelectric leg, I_{TE} is the current flow through the device, ε is the emittance, W is the perimeter of the side walls, and σ_{sb} is the Stefan-Boltzmann constant. The first term represents heat conduction, 2nd term the Thomson effect, third term the Joule heating, and the last term radiation heat loss from the side walls. We solve **Eq. (6)** numerically, using the measured values of the transport properties. The emittance of the electrodes and skutterudites were measured by FTIR (Fourier Transform Infrared) spectroscopy, and the values for the *n*-type, *p*-type, $CoSi_2$, and Co_2Si are 0.7, 0.6, 0.23 and 0.5, respectively. The solution of Eq. (6) leads to a temperature distribution, from which we can calculate the heat transfer Q_{Hot} and other properties used in the definitions of the effective properties [Eqs. (2-4)] as well as the device performance. We will compare the calculated properties with the measured effective properties and the device efficiency later.

3. Skutterudite Synthesis and Properties

The *n*- and *p*-type skutterudites are $Yb_{0.35}Co_4Sb_{12}$, and $NdFe_{3.5}Co_{0.5}Sb_{12}$, respectively. The skutterudites were alloyed from raw elements into polycrystalline skutterudites and then ball milled into a powder having nanosized grains.[23- 29] The powder was sintered by a direct current induced hot press process to produce a ½" diameter, 4 mm thick pellet. The pellet was cut in half to produce two 2 mm thick pellets; one would be used for the measurement of the thermal conductivity, and the other would be cut again into 2x2x12 mm bars for the measurement of the Seebeck coefficient and the electrical resistivity.

The temperature-dependant properties were measured as follows. The thermal diffusivity α and specific heat c_p are measured on Netzsch Instruments' laser flash (LFA 457) and differential scanning calorimeter (DSC 200 F3) systems, respectively. The thermal conductivity is obtained from $k = \alpha\ c_p\ \rho_m$, where the density, ρ_m, is measured by the Archimedes principle. The Seebeck coefficient and the electrical resistivity are measured with a commercially-available instrument (ZEM-3) made by ULVAC Technologies Inc. The thermal conductivity is measured in the direction perpendicular to the flat face of the pellet (cross-plane direction) and has a nominal uncertainty of 8%. Both the resistivity and the Seebeck coefficient are measured in the in-plane direction and have nominal uncertainty values of 8% and 5% respectively. The resulting uncertainty (root-sum-squares method) in *ZT* for the individual properties measurement is 14%. The property measurements are given in **figure 1**. The expected peak *ZT* of the *n*-type is 1.2 at 550 °C and of the *p*-type is 0.8 at 500 °C.

3.1. Device Pellet Fabrication

To build devices electrodes must be attached to *n*- and *p*-type skutterudites. In choosing electrode materials, the following factors should be taken into account: 1) the coefficient of

thermal expansion (CTE) should be well matched between the electrodes and skutterudites, 2) the electrodes should have high thermal and electrical conductivities relative to the skutterudites, 3) the bond should be mechanically strong and exhibit low electrical and thermal contact resistance, and 4) the bond should be chemically stable.

Based on the skutterudite CTEs and transport properties and through trials, we decided to use $CoSi_2$ for the *n*-type and Co_2Si for the *p*-type electrodes.[30] These electrodes are directly bonded onto the thermoelectric powder during hot pressing to produce device pellets. A major challenge was to optimize the press conditions to produce device pellets with good electrical properties that were free of cracks. To avoid cracking, we improved the temperature uniformity over the device pellet by reducing the diameter from ½" to ¼", and added electrically and thermally insulating plugs between the device pellet and the graphite plungers. Reducing the diameter had several practical advantages including: less bending stress on the electrodes and a smaller thermal time constant of the device pellet. The insulating plugs have a height of 7 mm and are made from a machinable glass (Macor) with a low thermal conductivity of 1.5 W/mK compared to graphite at 100 W/mK. Finite element analysis shows that the Macor plugs effectively insulate the device pellet from the high temperature graphite plungers so that the device pellet equilibrates to an almost uniform temperature with the die.[30] The plugs also redirect electrical current flow around the device pellet instead of through it. The *n*-type device pellets were pressed at a relatively high temperature and pressure of 750 °C and 84 MPa for 6 minutes to achieve a higher density and low contact resistance. The *p*-type pellets were pressed at a lower temperature and shorter time (675 °C at 98MPa for 3 minutes) to reduce mass diffusion at the interface and produce a smaller contact resistance.

After pressing, the device pellets were subsequently polished, inspected for cracks, and cut into legs. The legs were approximately 2x2 mm^2 in cross-sectional area, with a length of 4.7 mm comprising 3 mm length of skutterudite and 0.85 mm of electrode on each side. The

electrical resistance was measured at room temperature by a homebuilt 4-wire method. A sharp spring-loaded probe was mounted to a translation stage and scanned across the leg to measure the resistance versus length. Measurements were typically repeatable to length increments of about 2 μm. The bulk resistivity is extracted from the slope of the resistance curve within the skutterudite/electrode. A thin resistive layer formed at the skutterudite/electrode interface. The resistance across this layer is defined as the contact resistance. Each *p*-type interface has a contact resistance of 1.2-2.3 x 10^{-10} Ωm^2. The two interfaces combined contribute 1.5-2.9% of the total resistance of the leg. The *n*-type contact resistance is 0.7-2.0 x 10^{-10} Ωm^2 and contributes to 0.8-2.2% of the total resistance of the leg.

3. Experimental System

The experimental system was designed to measure ZT_{eff} and efficiency up to temperatures of 600 °C. We chose an inline unicouple configuration in which the legs are on the same axis instead of the conventional π-configuration to minimize thermal stress and thermal losses (**figure 2**). An axial force is applied to hold the legs in compression. Current and heat pass horizontally through the legs. Heat is generated in the middle at the heater assembly up to 600 °C while the ends are maintained near room temperature. The test is conducted in a cryostat in vacuum (<5x10^{-5} torr) to eliminate air conduction. Radiation at the heater and sides of the legs is the dominant mode of heat loss, which is carefully calibrated as described later. Cold water is passed through the cryostat cold finger to maintain the cold side temperature. There are five K-type thermocouples (2 mil diameter, bare), one on each electrode measuring T_{Cold1}, T_{Hot1}, T_{Cold2}, T_{Hot2} at a distance of 0.35 mm from the interface, and one at the heater measuring T_{heater}. The thermoelectric voltages V_{TE1}, V_{TE2}, V_{e1}, and V_{e2} were measured at each alumel thermocouple wire. The thermocouples were attached with Ag epoxy and cured at 120 °C for 8 hrs. To improve thermal contact Ag epoxy was used at the

hot electrode-Cu heater interface and In-Ga eutectic alloy at the cold electrode-Cu heat sink interface. At high temperature the organics of the Ag epoxy bake off, leaving a sintered Ag bond with relatively low electrical and thermal resistance.

The heater was designed to provide 6W at 600 °C. It is important that the heater assembly be as small as possible with small electrical leads to reduce heat loss. Platinum resistive thermometers (RTDs) serve as the heating elements. Two slots were milled in a 3x3x3 mm Cu block. A Pt RTD was inserted in each slot and backfilled with braze ($Ag_{45}Cu_{27}Zn_{25}Sn_3$ braze, T_{melt}=641-682 °C). Current was supplied by 2 mil Pt wire, 25 mm in length, which were brazed to the electrical leads of the RTDs.

Thermoelectric generator power output measurements require a variable load to best match the power. We use a current source as the variable load. When current flows through the device, referring to figure 2, voltages V_{TE1}, V_{TE2}, V_{e1}, V_{e2} were measured using the alumel arm of the thermocouple wires. The alumel wire is not a perfect electrode and must be compensated for its own Seebeck coefficient. The measured voltage was found by subtracting the Seebeck voltage of the alumel wire from the raw voltage. Note that V_{TE1} and V_{TE2} are generated by the Seebeck effect, while V_{e1} and V_{e2} are due to resistances between the electrodes and the copper heater block. Along the current flow direction, V_{TE1} and V_{TE2} are positive while V_{e1} and V_{e2} are negative. The heat entering the unicouple is given by

$$Q_{Hot} = IV_{heater} - Q_{Loss} + I_{TE}\left|V_{e1} + V_{e2}\right|, \quad (7)$$

where IV_{Heater} is the total electrical power dissipated by the RTD heating elements. The thermal losses between the T_{Hot1} and T_{Hot2} thermocouples are characterized by Q_{Loss}, which include: radiation from the Cu block/electrode surfaces, and conduction from two Pt wires and three thermocouples. The last term represents Joule heating created by the contact resistances between the Cu block and the thermoelectric legs. During the ZT_{eff} measurement I_{TE}=0.

The Q_{Loss} term is evaluated as follows. The heater assembly was calibrated for heat loss by

suspending it in vacuum and measuring the steady-state electric power needed to keep it at temperatures up to 625 °C. The Cu block surface was modelled as a grey body with a temperature-dependent emittance of the form $\varepsilon=\varepsilon_0+\varepsilon_T T_{heater}$ and fit to the experiments with a least squares regression ($\varepsilon_0=0.182$, $\varepsilon_T=7.9\cdot10^{-5}$). Heat losses from the thermocouples and Pt wires were calculated with a fin model with radiation as the major loss mechanism along the fin.[31]

4. Results and Discussion

Using the experimental system, we can measure the effective properties of each type of leg and the efficiency of a *p*-*n* unicouple. When measuring the effective properties of the same type of legs, we symmetrically place two legs—geometry as close to identical as possible—on both sides of the heater block. No current passes through the legs, $I_{TE}=0$. As heat is put into the heater through the RTDs and a temperature difference is established, the Seebeck voltage is measured using the thermocouple wires, from which the S_{eff} can be determined. The measured $\rho_{eff,}$ is determined by superimposing a small AC current through the legs and making a four point measurement. Current probes are located at the cold side of each leg and the thermocouples are used as the voltage probes as previously described. The measured ρ_{eff} is the combined resistance between the T_{Hot} and T_{Cold} locations, including the electrodes and contact resistances. The k_{eff} is determined by assuming heat input flows symmetrically to both sides of the legs. Thus, the measured ZT_{eff} includes bulk thermal and electrical resistances of 0.35 mm length of each electrode and its contact resistance with the skutterudite, and side wall heat loss from the electrode and skutterudite surfaces. These parasitic losses are also present in real devices.

Figure 3 plots the measured and calculated effective properties for the *n*-type and *p*-type legs. The “Eq. (6)” curves were based on solving Eq. (6), using the measured emittance and

transport properties. Error bars were calculated for each measurement point individually. Notice ρ_{eff} and k_{eff} have geometric parameters [Eqs. (3) and (4)] that introduce more uncertainty; while ZT_{eff} [Eq. (6)] does not have any geometric parameters. The magnitude of the measured *n*-type S_{eff} and ρ_{eff} are much higher than expected from individually measured *S(T)* and $\rho(T)$, but the power factor is similar (figure 3). This is likely due to a different carrier concentration between the device pellets and the pellets used in the individual property measurements. It is often observed that changes in pressing conditions can result in very different Seebeck coefficients and resistivities while producing similar power factors. **Figure 4a** plots ZT_{eff}, using effective properties in figure 3. The highest experimentally determined ZT_{eff} for the *n*-type was 0.74 (T_{Hot}=595 °C, T_{Cold}=52 °C), and for the *p*-type was 0.51 (T_{Hot}=600 °C, T_{Cold}=77 °C). In the same figure, we also show two theoretical curves for each type of skutterudite. The "Eq. (6)" curves were calculated by solving Eq. (6), including radiation loss from side walls and resistances of the electrodes. The "no losses" curves neglect radiation loss and losses due to the electrodes. In figure 4b, we show calculated efficiency of each type of legs using three approaches. One is based on Eq. (1) using the experimentally determined ZT_{eff} to replace *ZT*. The two other efficiency curves are based on solving Eq. (6), one includes radiation and electrodes losses (curve labelled "Eq. (6)") and the other does not ("no losses"), similar to the conditions in figure 4(a). The figure shows that efficiency values obtained from Eq. (1) using experimentally determined ZT_{eff} are close to that obtained from solving Eq. (6).

During the efficiency measurement, a current is passed through the unicouple (figure 2), electrical power is generated in the legs and dissipated at the heater assembly. **Figure 5** shows measured power [5(a)] and corresponding efficiency values [5(b)]. During the test the *n*- and *p*-type legs operated between 558-559 °C and 544-546 °C, on the hot side and 58-63 °C and 76-83 °C on the cold side, respectively. The maximum measured power was 0.445 W at 6 A. Several efficiency values are plotted. The "raw" efficiency curve is based on power

from the total external voltage,

$$P_e = I_{TE} \bullet \left(V_{TE1} + V_{e1} + V_{e2} + V_{TE2}\right), \quad (8)$$

while heat leakage from the heater block, Q_{Loss}, is omitted such that $Q_{Hot} = IV_{Heater}$. The efficiency is simply calculated as $\eta = P_e / Q_{hot}$. The "uncorrected heat loss" points are obtained by computing the power output based on measured V_{TE1} and V_{TE2} only,

$$P_e = I_{TE} \bullet V_{TE1} + I_{TE} \bullet V_{TE2}, \quad (9)$$

and

$$Q_{Hot} = IV_{Heater} + I_{TE}\left|V_{e1} + V_{e2}\right|. \quad (10)$$

This includes heat dissipated at the RTD and heater assembly but does not account for the heat leakage from the heater block. The "meas." points use the power from **Eq. (9)** and the hot side heat transfer from **Eq. (7)**; it is the most accurate characterization of device performance. The maximum efficiency thus obtained was 9.1% at 5 A (figure 5a). The "Eq. (6)" curve was calculated based on solving Eq. (6), including radiation and electrodes losses. Figure 5a also shows the power of the individual legs which peaks at very different current values, indicating that the geometry is not well matched to maximize either efficiency or power of the unicouple. Our model predicts that the maximum efficiency will increase from 9.0% to 9.2% if the cross sectional area of the *n*-type leg is decreased to 0.9 times its present value and the *p*-type leg is increased to 1.3 times its present value. Thus the efficiency of this unicouple is relatively insensitive to geometry matching and current matching errors.

5. Conclusion

We developed a device testing system for a mid-temperature thermoelectric unicouple up to 600 °C. Small leg geometries were used in an inline configuration to reduce thermal stress and heat loss. This setup enables measurement of the effective thermoelectric properties,

ZT_{eff}, and efficiency while working under a large temperature difference.

The testing system is employed to characterize skutterudites. $CoSi_2$ and Co_2Si were chosen as the *n*- and *p*-type electrodes, respectively, and they were directly bonded onto skutterudites during the hot pressing process. We demonstrated ZT_{eff}=0.74 for the *n*-type operating between 52 °C and 595 °C, and ZT_{eff}=0.51 for the *p*-type operating between 77 °C and 600 °C. The maximum efficiency of the *p-n* unicouple was determined to be 9.1% operating between ~70 °C and 550 °C. The efficiency measured is among the highest of skutterudites, suggesting their promising future in energy harvesting applications.

Acknowledgements

This material is partially based upon work supported as part of the Solid State Solar-Thermal Energy Conversion Center (S^3TEC), an Energy Frontier Research Center funded by the U.S. Department of Energy, Office of Science, and Office of Basic Energy Sciences under Award Number: DE-SC0001299/DE-FG02-09ER46577 (G.C. and Z.F.R.) and MIT-KFUPM Clean Water and Clean Energy Center (A.M.)

Received: ((will be filled in by the editorial staff))
Revised: ((will be filled in by the editorial staff))
Published online: ((will be filled in by the editorial staff))

1 T.Hendricks, *Engineering Scoping Study of Thermoelectric Generator Systems for Industrial Waste Heat Recovery*.
2 J. Yang, and F. Stabler, *Journal of Electronic Materials*, 2009, **38**, 7.
3 D. Kraemer, B. Poudel, H.P. Feng, J.C. Caylor, B. Yu, X. Yan, Y. Ma, X.W. Wang, D. Wang, A. Muto, K. McEnaney, M. Chiesa, Z.F. Ren, and G. Chen, *Nat. Mater.*, 2011, **10**, 532-538.
4 P. Tomeš, C. Suter, M. Trottmann, A. Steinfeld, and A. Weidenkaff, *J. Mater. Res.*, 2011, **26**, 15.
5 H. Goldsmid, *Electronic Refrigeration*, Pion Limited: London, 1986.
6 T. Caillat, J. Fleurial, G. Snyder, A. Zoltan, D. Zoltan, and A. Borshchevsky, *ICT Proceedings*, 1999, 473-476.
7 T. Caillat, J. Fleurial, G. Snyder, and A. Borshchevsky,. *ICT Proceeding*, 2001, 282-285
8 J. Yang, and T. Caillat,. *MRS Bulletin*, 2006, **31**, 224-229.
9 M. Kambe, T. Jinushi, and Z. Ishijima, *J. Electronic Materials*, 2010, **39**, 9.
10 J. D'Angelo, E. Case, N. Matchanov, C. Wu, T. Hogan, J. Barnard, C. Cauchy, T. Hendricks, and M. Kanatzidis, *Journal of Electronic Materials*, 2011, **40**, 10
11 K. Salzgeber, P. Prenninger, A. Grytsiv, P. Rogl, and E. Bauer, *Journal of Elec Mat.*, 2009, **39**, 2074-2078.
12 M. El-Genk, H. Saber, T. Caillat, and J. Sakamoto, *Energy Conversion and Management*, 2006, **47**, 174-200.
13 M. El-Genk, H. Saber, and T. Caillat, *AIP Conf. Proc.*, 2004, **699**, 541-552.
14 H. Saber, M. El-Genk, and T. Caillat, *AIP Conf. Proc.*, 2005, **746**, 584-592.
15 H. Saber, and M. El-Genk, *Energy Conversion and Management*, 2007, **48**, 1383-1400.

16 Z. Gu, Y. Han, F. Pan, X. Wang, D. Weng and S. Zhou, *Materials Science Forum*, 2009, 610 - 613, 389-393.
17 D. Zhao, X. Li, L. He, W. Jiang, and L. Chen,. *Journal of Alloys and Compounds*, 2009, **477**, 425-431.
18 J. Fan, L. Chen, S. Bai, and X. Shi, *Materials Letters*, 2004, **58**, 3876-3878.
19 X. Li, L. Chen, J. Fan and S. Bai, ICT 2005 Proc., 2005, 540- 542.
20 D. Zhaoa, C. Tiana, S. Tanga, Y. Liua, L. Jianga, L. Chen, *Materials Science in Semiconductor Processing*, 2010, **13**, 221-224.
21 A. Muto, D. Kraemer, Q. Hao, Z. Ren, and G. Chen, *Review of Scientific Instruments* , 2009, **80**, 7.
22 A. Muto, D. Kraemer, Q. Hao, Z. Ren, and G. Chen, *Review of Scientific Instruments* , 2009, **80**, 7.
23 J. Yang, *PhD*, Boston College, Jun. **2010**.
24 A. Minnich, M. Dresselhaus, Z. Ren, and G.Chen., *Energy Environ. Sci.*, 2009, **2**, 466 - 479.
25 A. Minnich, H. Lee, X. Wang, G. Joshi, M. Dresselhaus, Z. Ren, G. Chen, and D. Vashaee, *Phys. Rev. B*, 2009, **80**, 155327
26 M. Dresselhaus, G. Chen, M. Tang, R. Yang, H. Lee, Z. Wang, Z. Ren, J. Fleurial, and P. Gogna, *Advanced Materials*, 2007, **19**, 1043-1053.
27 X. Wang, H. Lee, Y. Lan, G. Zhu, G. Joshi, D. Wang, J. Yang, A. Muto, M. Y. Tang, J. Klatsky, S. Song, M. Dresselhaus, G. Chen, and Z. Ren. *Applied Physics Letters*, 2008, **93**, 3.
28 B. Poudel, Q. Hao, Y. Ma, Y. Lan, A. Minnich, B. Yu, X. Yan, D. Wang, A. Muto, D. Vashaee, X. Chen, J. Liu, M. Dresselhaus, G. Chen, and Z. Ren, *Science*, 2008, **320**, 634-638.
29 J. Yang, Q. Hao, H. Wang, Y. Lan, Q. He, A. Minnich, D. Wang, J. Harriman, V. Varki, M. Dresselhaus, G. Chen, *PHYSICAL REVIEW B*, 2009, **80**, 115329.
30 A. Muto, *PhD*, MIT, Sept. **2011**
31 T. Bergman, A. Levine, F. Incropera, D.Dewitt, Fundamentals of Heat and Mass Transfer, John Wiley and Sons Inc., 2011

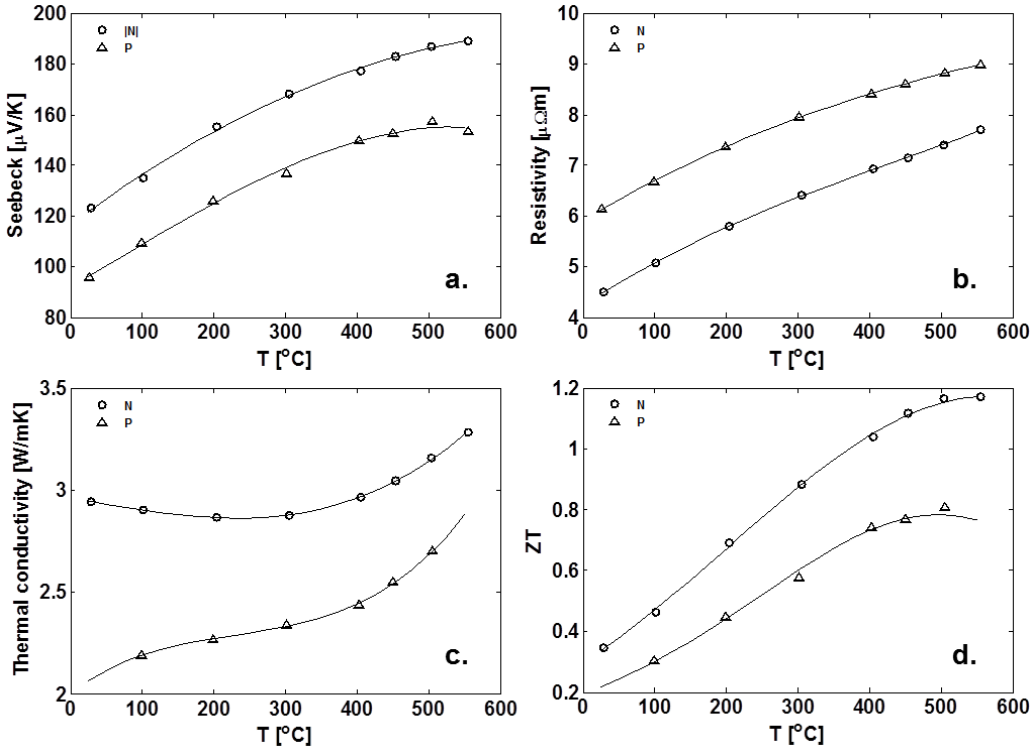

Figure 1. Measured skutterudite properties. Points represent measured values, lines are polynomial fits. Notice that the absolute value of the *n*-type Seebeck coefficient is plotted.

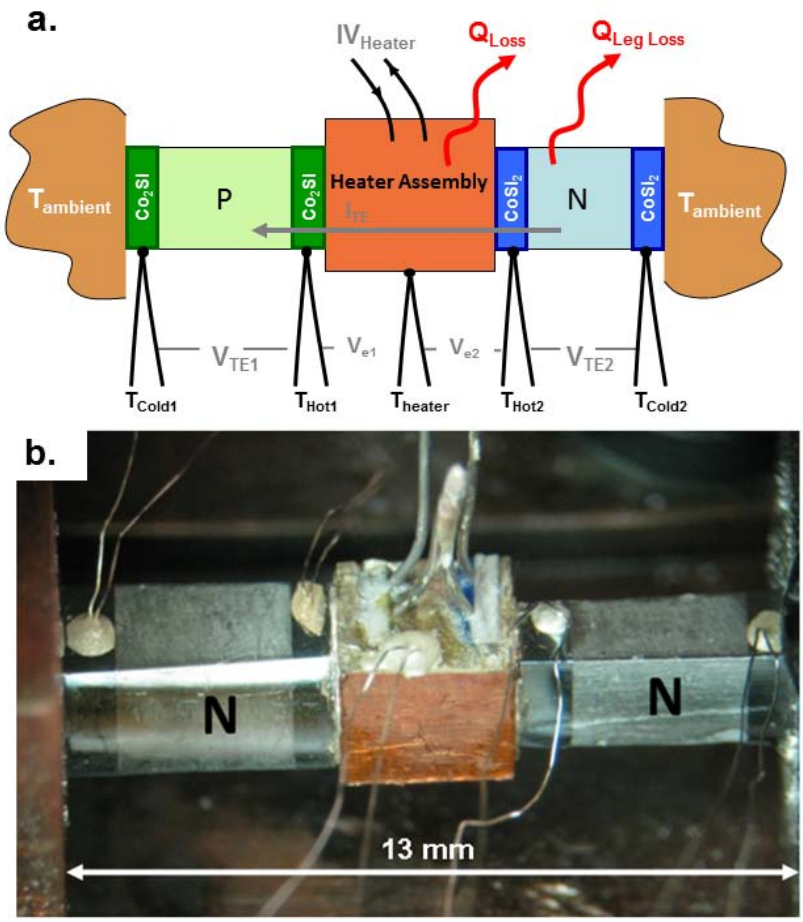

Figure 2. Unicouple with the inline configuration. (a) Schematic of the *p*-*n* unicouple during the efficiency measurement. The thermoelectric voltage is measured at the alumel wires between K-type thermocouples. (b) Photograph of *n*-*n* effective properties measurement.

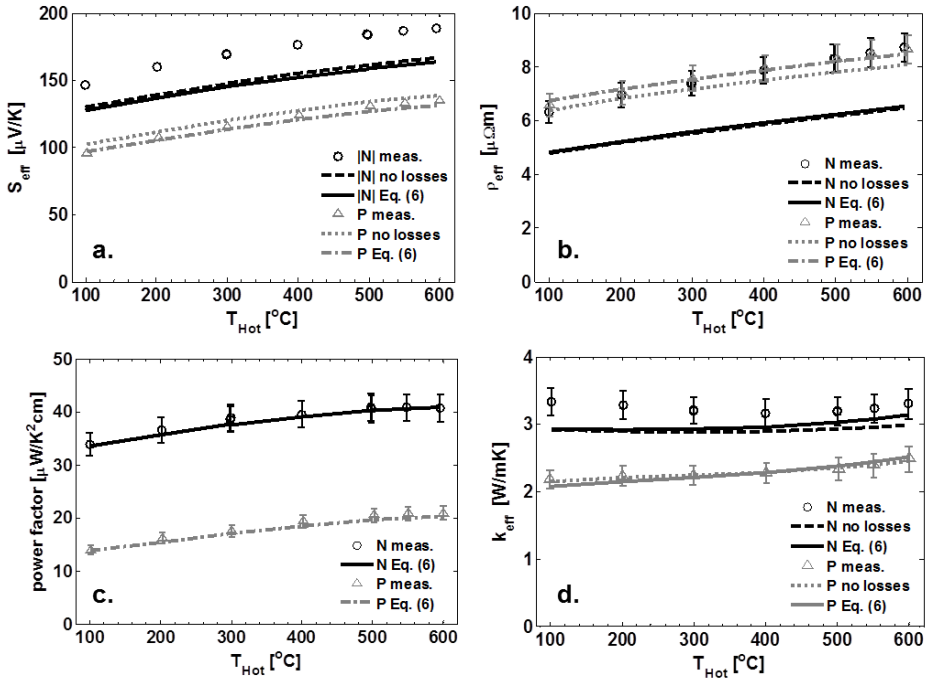

Figure 3. Effective properties of the *n*- and *p*-type. Points with error bars are measured values, "Eq. (6)" curves are based on solving Eq. (6) with parasitic losses (neglecting contact resistance) from the electrodes and side walls of the legs, and "no losses" curves do not include parasitic losses.

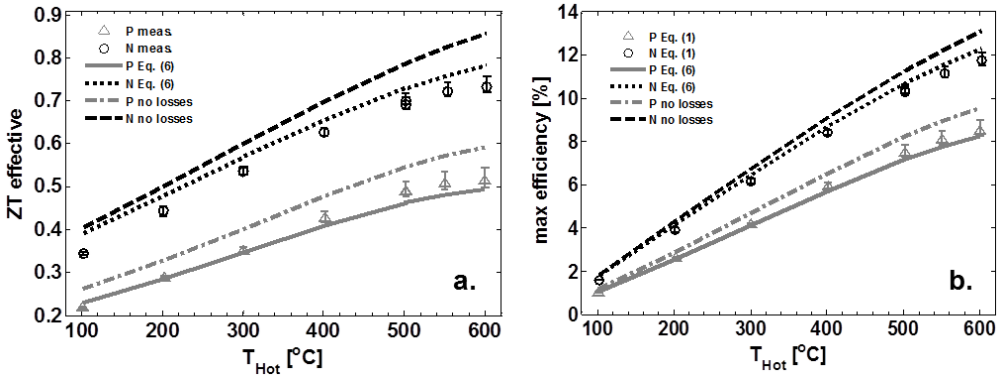

Figure 4. (a) Effective *ZT* of the *n*- and *p*-type. Points are the measured values, "Eq. (6)" curves are based on solving Eq. (6) with parasitic losses (neglecting contact resistance) from the electrodes and side walls of the legs, and "no losses" curves do not include parasitic losses. (b) Points are maximum efficiency calculated from measured ZT_{eff} using Eq. (1).

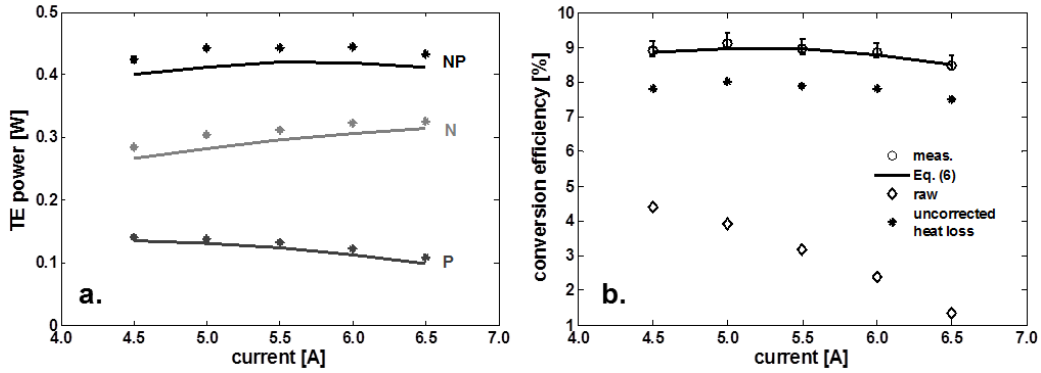

Figure. 5 (a) Power versus current for *n*- and *p*- legs individually and summed together. Points are measured values, lines are calculated from Eq. (6). (b) Conversion efficiency versus current. Points marked "raw" are based on the total measured voltage across the couple and the power input to the RTD heaters. The "uncorrected heat loss" points are obtained using Eq. (9) for power output and **Eq. (10)** for heat input. The "meas." points are the most accurate characterization of performance they are obtained using Eq. (9) for power output and Eq. (7) for the heat input.